Acta Acustica 2023, **7**, 30

https://doi.org/10.1051/aacus/2023024

Available online at:
https://acta-acustica.edpsciences.org

SCIENTIFIC ARTICLE OPEN ACCESS

Numerical study of beam shape adaptation by anisotropic disk covering transducer or metamaterial

Nico F. Declercq*

Georgia Institute of Technology, George W. Woodruff School of Mechanical Engineering, Georgia Tech Europe, Laboratory for Ultrasonic Nondestructive Evaluation, IRL 2958 Georgia Tech – CNRS, 2 rue Marconi, 57070 Metz, France

Received 20 January 2023, Accepted 22 May 2023

Abstract – Metamaterials are intensely explored for their capabilities to modify sound beams. In addition to frequency filtering, acoustic lenses offer intriguing possibilities for shaping sound beams. For the time being, the versatility of metamaterials remains limitless. In beam-shape adaptation, however, their complexity suggests that manufacturers of transducers could benefit from combining metamaterials with more conventional materials. This paper investigates the transmission of a circumscribed beam through a stratum of anisotropic material to examine the change in beam shape after transmission. The incident sound is presumed to originate from a conventional transducer, possibly coated with a metamaterial to modify the sound field, before being transmitted through the anisotropic layer. Different incident beam shapes, such as conical-like, Gaussian, and pillar beams, are investigated. While the results are not exhaustive, they demonstrate the beam shape's adaptability.

Keywords: Beam shape adaptation, Gaussian beams, Pillar beams, Conical-like beams, Fiber-reinforced composites, Metamaterials

1 Introduction

Recently, it has been demonstrated that metasurfaces are efficient and compact structures for designing arbitrary wavefronts. Metasurfaces are planar metamaterials with a subwavelength thickness that enables wavefront sculpting by introducing gradients in the spatial wave response of these flat structures. Impedance-based holographic acoustic lenses have been developed [1] to transform the sound output from a transducer into the desired field for medical applications [2]. Bessel beams, known for their diffraction resilience, can be formed equally by a metamaterial placed before a transducer [3]. The focus can be adjusted by shifting one material to another, covering the transducer surface [4]. Acoustic gradient-index (GRIN) metasurfaces, engineered from soft graded-porous silicone rubber, also permit beam steering and focusing [5]. Acoustic metamaterials are also developed for making a Mikaelian lens [6] or coding acoustic waves by sending them through the metamaterial before transmission [7]. Certain metamaterials achieve anisotropic behavior but not in the homogenized sense of actual crystals or fiber-reinforced composites with constituents way below the involved acoustic wavelengths [8]. Embedded in-plate applications also exist in which metamaterials steer or focus beams [9].

The versatility of metamaterials remains limitless for the time being. In beam-shape modifications, however, the degree of complexity implies that transducer manufacturers might gain from merging metamaterials with traditional substances, if possible. Those substances can be crystals or fiber-reinforced composites, anisotropic but homogeneous for the involved sound waves. Emitting sound through such conventional materials can further adjust beams without sophistication, and, therefore, find applications in the above-mentioned topics of beam-shape, steering and focus adjustments in the medical field.

It is known that sound transmits through crystals in a directional-dependent manner. However, the effect on beam shape, merely due to anisotropy and not due to impedance inhomogeneity, usually is not considered. Here, we investigate the transmission of acoustic beams perpendicularly incident on an anisotropic plate. The 3D beams are modeled by a plane wave expansion based on a Fourier series approach whereby each constituting plane wave interacts with the plate under consideration.

That sound is sensitive to the anisotropic linear stiffness of composites and has been widely exploited in the past. Indeed, ultrasonic investigation of fiber-reinforced composites' stiffnesses is based on straightforward principles involving Snell's law, Newton's laws, Hooke's law, and the continuity of mechanical strains and stresses at the involved interfaces between composite layers or the surrounding

*Corresponding author: declercq@gatech.edu

water. Linear stiffness determination is practically achieved by exploiting direction dependence in experiments. It is, therefore, somewhat different from damage detection using C-scans or guided waves [10–13] or non-linear acoustics [14]. Breakthroughs came from the team of Dale Chimenti [15–20] and others [21–23]. A direct method to probe the stiffness of composites is based on multiple-angle incidence, done in the form of a transducer rotation along a sphere [24] or through focused sound with the help of phased array technology [25, 26] or otherwise [19, 27–29]. A significant challenge is to work on an air-coupled system [30, 31], which is not addressed in the current paper. In the last decades, the extensive use of fiber-reinforced composites forced researchers to develop novel and practical techniques to realize nondestructive testing (NDT) on those materials. Such evolution is continuing today [32–35].

Understanding sound transmission through an anisotropic layer and how an acoustic beam deforms by it can be done in the same framework as studies aimed at nondestructive testing. It has been shown before by Rehman et al. [36] that the reflected beam pattern may reveal properties of composites. They showed that reflected Gaussian beams are only sensitive to material properties if oblique incidence is considered. The current work shows that the oblique incidence is not a requirement. Transmitted beams, for normal incidence, are sensitive to composites' internal structure.

Even though the current work reveals a proof of concept and is numerical, it is essential to note what type of measurements could be performed by experimentalists for further investigations. One may, for instance, apply a needle transducer [37] as a receiver and perform a point-by-point scan of the transmitted sound beam. The needle may be piezoelectric or a metal-coated fiber tip paired with a heterodyne interferometer that senses an optical path alteration caused by the fiber tip's oscillation in the sound field [38]. Alternatively, a single-mode fiber-optic probe hydrophone (FOPH) can be used for local sound measurements [39], or Acousto-optic diffraction can also be applied to measure a sound field [40]. The latter typically comprises a global measurement of the entire beam and is insufficiently resolved for point-by-point information. Tomographic variations of acousto-optic Bragg diffraction [41–47] can approach an adaptation of acousto-optics to point-by-point measurements [48, 49] and Schlieren imaging [50, 51–56].

2 Incident beam descriptions

One may hardly imagine what sort of beams will be manufactured in future developments in metamaterials. As proof of concept, three types of 3D beams are assumed in this research: *Gaussian beams*, *pillar beams*, and *conical-like beams*.

Pillar beams look like a filled cylinders. The conical-like beams studied here have beam flanks showing exponential decay. There is a particular reason for this choice. The beauty of conical-like beams is that they possess properties similar to inhomogeneous waves. It is well known [57] that the propagation features of inhomogeneous waves in crystals depend not only on the direction of propagation but also on the value of the inhomogeneity vector. Therefore, whereas classical homogeneous plane waves cannot reflect composites' internal symmetry for normal incidence, inhomogeneous waves are susceptible to symmetry because rotating the inhomogeneity vector (for normal incidence) must result in different propagation properties. A conical-like beam contains inhomogeneity properties for each radial direction and may reflect the fundamental in-plane symmetry at once; therefore, it is worthwhile considering.

A Gaussian beam $G(x,\ y,\ z)$, is characterized by its profile at $z = 0$ as

$$G(x,y,0) = \exp\left[-\left[\frac{\sqrt{x^2+y^2}}{W}\right]^2\right], \tag{1}$$

whereas a conical-like beam $C(x,\ y,\ z)$ by

$$C(x,y,0) = \exp\left(-\beta\left|\sqrt{x^2+y^2}\right|\right) \tag{2}$$

and a pillar beam $P(x,\ y,\ z)$ by

$$P(x,y,0) = \exp\left[-\left[\frac{\sqrt{x^2+y^2}}{W}\right]^{64}\right]. \tag{3}$$

In order to compare the different beams, we enforce the same amount of energy, whence

$$\begin{aligned}\int_{-\infty}^{+\infty}\int_{-\infty}^{+\infty} G^2\mathrm{d}x\mathrm{d}y &= \int_{-\infty}^{+\infty}\int_{-\infty}^{+\infty} C^2\mathrm{d}x\mathrm{d}y \\ &= \int_{-\infty}^{+\infty}\int_{-\infty}^{+\infty} P^2\mathrm{d}x\mathrm{d}y.\end{aligned} \tag{4}$$

Because of the symmetry of the considered profiles, i.e., each profile $K(x,\ y,\ 0) = K(R)$ with $R = \sqrt{x^2+y^2}$ the radius, equation (4) are equivalent to

$$\int_0^{+\infty} G^2\mathrm{d}R = \int_0^{+\infty} C^2\mathrm{d}R = \int_0^{+\infty} P^2\mathrm{d}R \simeq B. \tag{5}$$

Therefore

$$W = \frac{\sqrt{2}}{\sqrt{\pi}\beta} \quad \text{and} \quad B = \frac{\sqrt{2\pi}}{4}W. \tag{6}$$

Modeling ultrasound beams is done by Fourier analysis, where each beam is a sum of plane waves. Therefore, the transmitted beam is the sum of all transmitted plane waves originating from the plane waves constituting the perpendicular incident beam. The interaction of plane waves with an anisotropic layer is discussed in Section 3.

3 Sound transmission

Coupling a transducer, with or without a metamaterial in between, to an anisotropic disk could be done in different ways. The current paper merely focuses on the effect caused by the anisotropic material and assumes liquid coupling. It is also assumed that the transmitted beam arises on the

opposite side of the disk in a liquid. The liquid in both cases is water, with a speed of sound of 1480 m/s and a density of 1000 kg/m^3. We also assume that the disk is large enough so the reflections from its edges do not occur, an assumption that makes sense in the case of perpendicular incident bounded beams. The material is considered orthotropic, typical for fiber-reinforced composites.

The interaction of sound with an anisotropic layer is well-described in the literature [58–61]. A summary follows.

3.1 Material description

With Einstein's double suffix notation convention, the dynamics of an anisotropic material is described [20, 62] by

$$\frac{\partial \sigma_{ij}}{\partial r_j} = \rho \frac{\partial^2 u_i}{\partial t^2}. \tag{7}$$

With $i, j = 1, 2, 3$, and σ_{ij} being the stress tensor, and $\boldsymbol{u}$ the particle displacement. $\boldsymbol{r}$ is the position and t is time.

Hooke's law, is given by

$$\begin{bmatrix} \sigma_{11} \\ \sigma_{22} \\ \sigma_{33} \\ \sigma_{23} \\ \sigma_{13} \\ \sigma_{12} \end{bmatrix} = \begin{bmatrix} C_{11} & C_{12} & C_{13} & C_{14} & C_{15} & C_{16} \\ C_{12} & C_{22} & C_{23} & C_{24} & C_{25} & C_{26} \\ C_{13} & C_{23} & C_{33} & C_{34} & C_{35} & C_{36} \\ C_{14} & C_{24} & C_{34} & C_{44} & C_{45} & C_{46} \\ C_{15} & C_{25} & C_{35} & C_{45} & C_{55} & C_{56} \\ C_{16} & C_{26} & C_{36} & C_{46} & C_{56} & C_{66} \end{bmatrix} \times \begin{bmatrix} e_{11} \\ e_{22} \\ e_{33} \\ 2e_{23} \\ 2e_{13} \\ 2e_{12} \end{bmatrix}. \tag{8}$$

Orthotropy considerations [20, 62] result in

$$\begin{aligned} C_{14} = C_{24} = C_{34} = C_{15} = C_{25} = C_{35} = C_{16} = C_{26} \\ = C_{36} = C_{45} = C_{46} = C_{56} = 0. \end{aligned} \tag{9}$$

The stiffness constants of orthotropic materials are related to the Engineering constants, with Young's moduli E_{11}, E_{22} and E_{33}, the Poisson coefficients ν_{23}, ν_{13} and ν_{12}, and the shear moduli G_{23}, G_{13} and G_{12}. The connection is

$$\begin{bmatrix} C_{11} & C_{12} & C_{13} & 0 & 0 & 0 \\ C_{12} & C_{22} & C_{23} & 0 & 0 & 0 \\ C_{13} & C_{23} & C_{33} & 0 & 0 & 0 \\ 0 & 0 & 0 & C_{44} & 0 & 0 \\ 0 & 0 & 0 & 0 & C_{55} & 0 \\ 0 & 0 & 0 & 0 & 0 & C_{66} \end{bmatrix} = \begin{bmatrix} 1/E_{11} & -\nu_{12}/E_{11} & -\nu_{13}/E_{11} & 0 & 0 & 0 \\ -\nu_{21}/E_{22} & 1/E_{22} & -\nu_{23}/E_{22} & 0 & 0 & 0 \\ -\nu_{31}/E_{33} & -\nu_{32}/E_{33} & 1/E_{33} & 0 & 0 & 0 \\ 0 & 0 & 0 & 1/G_{23} & 0 & 0 \\ 0 & 0 & 0 & 0 & 1/G_{31} & 0 \\ 0 & 0 & 0 & 0 & 0 & 1/G_{12} \end{bmatrix}^{-1} \tag{10}$$

Table 1. Properties of a Carbon/Epoxy unidirectional fiber-reinforced composites plate assumed as the material used for the 3 mm disk through which each sound beam passes.

Parameter	Value
ρ [kg/m^3]	1525
E_{11} [MPa]	119 130 × (1 – 0.0025i)
E_{22} [MPa]	8850 × (1 – 0.03i)
E_{33} [MPa]	10 000 × (1 – 0.03i)
ν_{23}	0.475 × (1 – 0.015i)
ν_{13}	0.275 × (1 – 0.01i)
ν_{12}	0.306 × (1 – 0.01i)
G_{23} [MPa]	3000 × (1 – 0.05i)
G_{13} [MPa]	5000 × (1 – 0.02i)
G_{12} [MPa]	5500 × (1 – 0.03i)

with

$$\nu_{32} = \nu_{23} \frac{E_{33}}{E_{22}}, \tag{11}$$

$$\nu_{31} = \nu_{13} \frac{E_{33}}{E_{11}}, \tag{12}$$

$$\nu_{21} = \nu_{12} \frac{E_{22}}{E_{11}}, \tag{13}$$

and

$$G_{ij} = G_{ji}. \tag{14}$$

The reverse Voigt procedure transforms the stiffness tensor C_{mn} of rank 2 to the stiffness tensor c_{ijkl} of rank 4 as (1→11), (2→22), (3→33), (4→23 = 32), (5→13 = 31) and (6→12 = 21), after which we can conveniently rotate the composite as needed for the different plane waves constituting a bounded beam. A rotation R transforms the intrinsic stiffness constants $c_{ijkl} = c^I_{ijkl}$ into stiffness constants $c_{ijkl} = c^R_{ijkl}$ in coordinates corresponding to a rotated (laboratory) system as follows:

$$c^R_{ijkl} = R_{im} R_{jn} R_{kp} R_{lq} c^I_{mnpq}, \tag{15}$$

where R_{ij} are the entries of the rotation matrix for a rotation from the intrinsic lattice coordinate system to the laboratory coordinate system.

Equation (7) then becomes

$$\rho \frac{\partial^2 u_i}{\partial t^2} = c_{ijkl} \frac{\partial^2 u_l}{\partial x_j \partial x_k}. \tag{16}$$

A plane wave solution of (16) is of the form

$$u_i = U_i \exp i\left[n_j r_j - \omega t\right], \tag{17}$$

where $\boldsymbol{n}$ is the wave vector. If this is entered in (16), straightforward calculations result in

$$\left[\frac{1}{\rho} c_{ijkl} n_k n_j - \omega^2 \delta_{il}\right] U_l = 0. \tag{18}$$

Equation (18) is called the Christoffel equation [20, 62]. It relates the slowness $\boldsymbol{n}/\omega$ and the polarization $\boldsymbol{U}$ to the

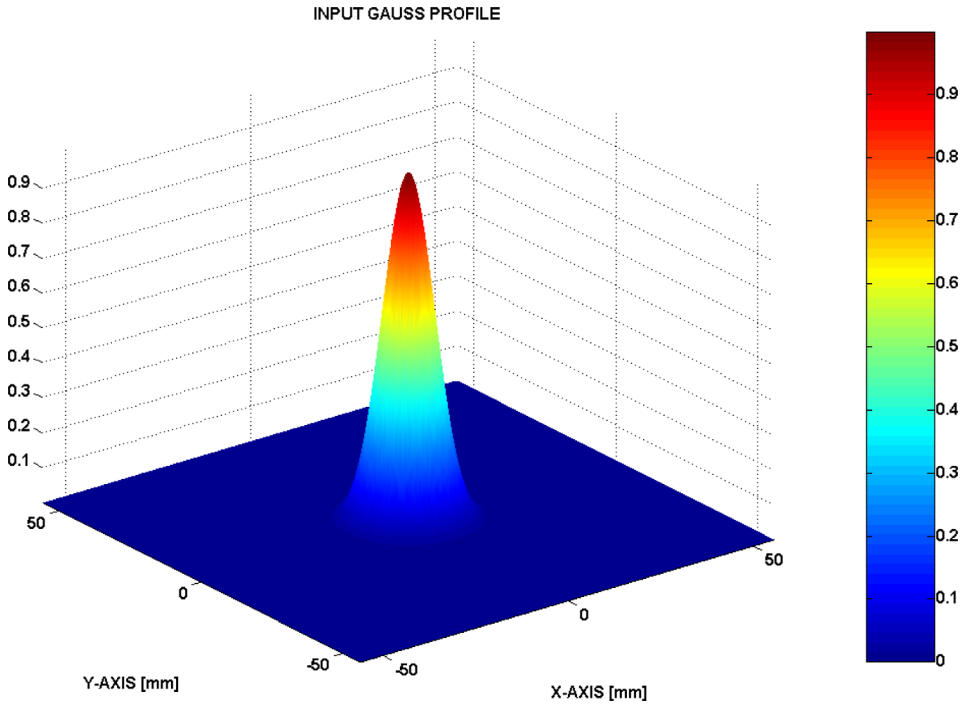

Fig. 1. Profile of an incident *Gaussian beam*, having the same amount of energy as a *conical-like beam*, shown in Figure 2, for $\beta = 100/\text{m}$.

propagation direction and is solved by assuming nontrivial solutions, followed by the determination of the corresponding eigenvectors.

3.2 Plane wave interactions with interfaces

Apart from the above determined Christoffel's equation which is comparable to a dispersion relation for isotropic media, we must account for Snell's law to determine the wave vector components along the interface, as well as the continuity condition.

3.2.a Snell's law

If sound inside the bulk of the composite laminate results from impinging plane waves (denoted by superscript "inc"), Snell's law for interfaces perpendicular to n_3, states that

$$n_1 = n_1^{\text{inc}} \quad \text{and} \quad n_2 = n_2^{\text{inc}}. \tag{19}$$

Then, requiring nontrivial solutions, (18) leads to a sixth-degree polynomial equation of the form

$$(n_3)^6 + B_5(n_3)^5 + A_4(n_3)^4 + B_3(n_3)^3 + A_2(n_3)^2 + B_1(n_3)^1 + A_0 = 0. \tag{20}$$

Furthermore, symmetry higher than or equal to monoclinic symmetry results in

$$B_j = 0, \tag{21}$$

whence three independent solutions for n_3 are found.

3.2.b Continuity of normal stress and displacement

For a plate, continuity of normal stress and normal displacement is required along the water-solid interface,

$$u_3^{\text{water}} = u_3^{\text{solid}} \tag{22}$$

and

$$\sigma_{i3}^{\text{water}} = \sigma_{i3}^{\text{solid}}, \quad i = 1, 2, 3. \tag{23}$$

4 Numerical results

Each of the considered beams, i.e. *Gaussian*, *pillar* and *conical-like*, is decomposed into many harmonic homogeneous plane waves by a 2D Fast Fourier Transform (FFT). The FFT is taken on the interval $[-7\text{W}, 7\text{W}]^2$ on 2^{2N} equally distributed samples, for N the smallest positive integer for which

$$2^{2N} \geq 168/W \tag{24}$$

and W is expressed in [m]. The number of samples equals the number of waves in the plane wave decomposition of the considered beam, and the considered interval is sufficiently extended to ensure reliable simulations.

This paper's numerical simulations are based on calculating the transmission coefficient for every plane wave constituting the incident beam.

The considered composite has a thickness of 3 mm and consists of one layer of unidirectional material – carbon fibers in epoxy. The elastic properties of such material are

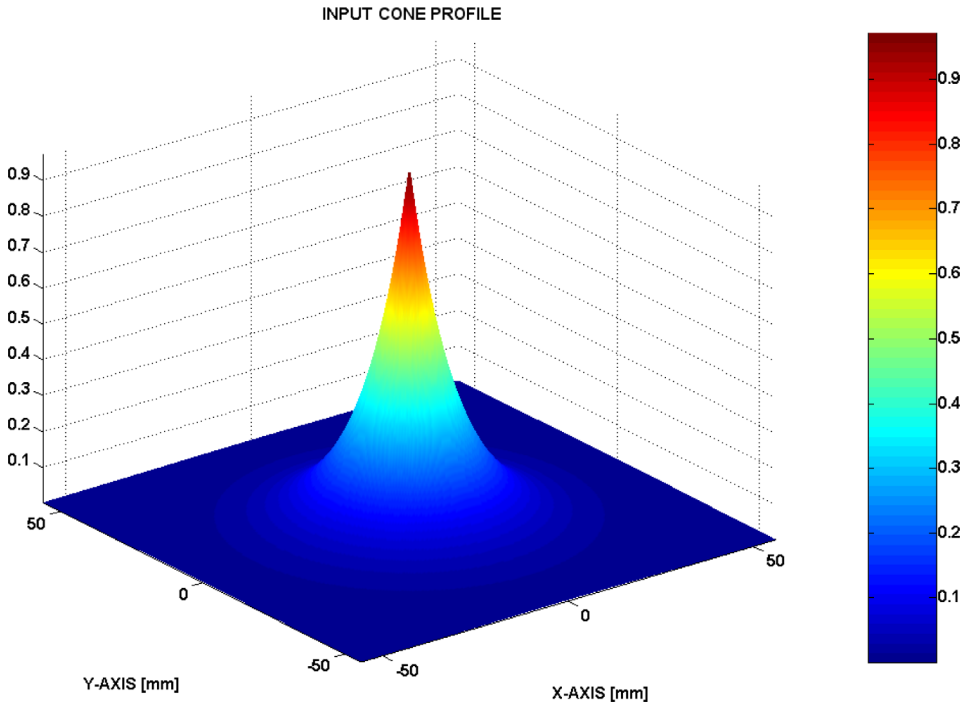

Fig. 2. Profile of a *conical-like beam* for $\beta = 100/\text{m}$. This beam shows remarkable resemblance with an inhomogeneous wave. Its amplitude diminishes exponentially from the center of the beam.

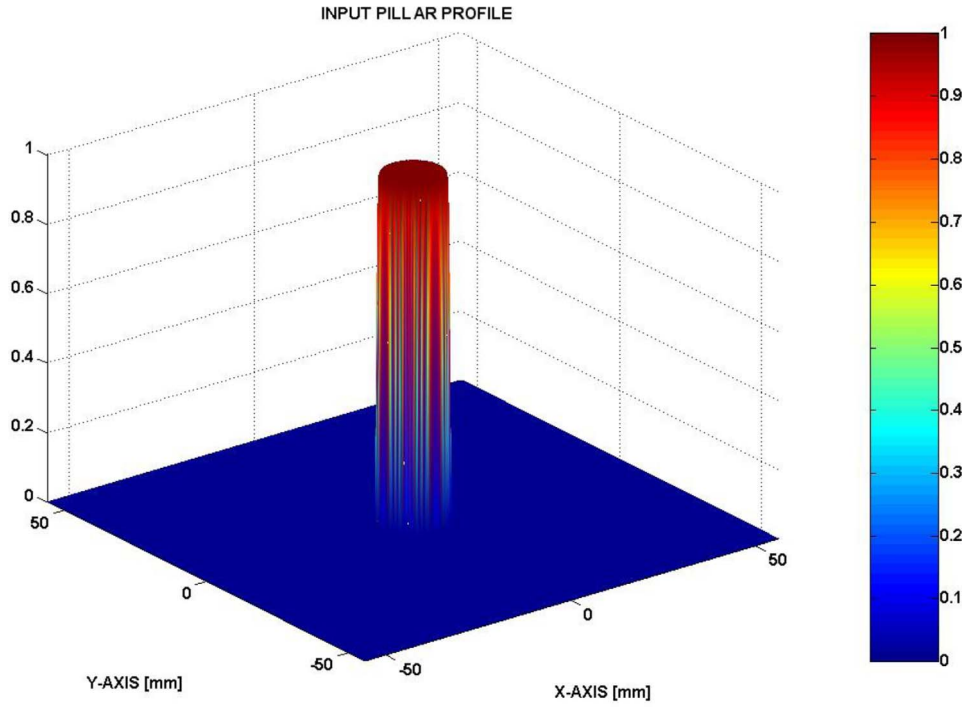

Fig. 3. Profile of an incident *pillar beam*, having the same amount of energy as a *conical-like beam*, shown in Figure 2, for $\beta = 100/\text{m}$.

given in Table 1. The fibers are directed in the XY-plane along the X-direction. Therefore, the material is stiffer along the X-direction than the Y-direction [10].

Figure 1 shows the profile of an incident *Gaussian beam*, having the same amount of energy as a *conical-like beam*, shown in Figure 2, for $\beta = 100/\text{m}$. The comparative *pillar beam* is given in Figure 3. We only discuss transmitted beam profiles because that is this paper's purpose.

Figure 4 shows the transmitted beam profile for an incident *Gaussian beam* with the same amount of energy as a

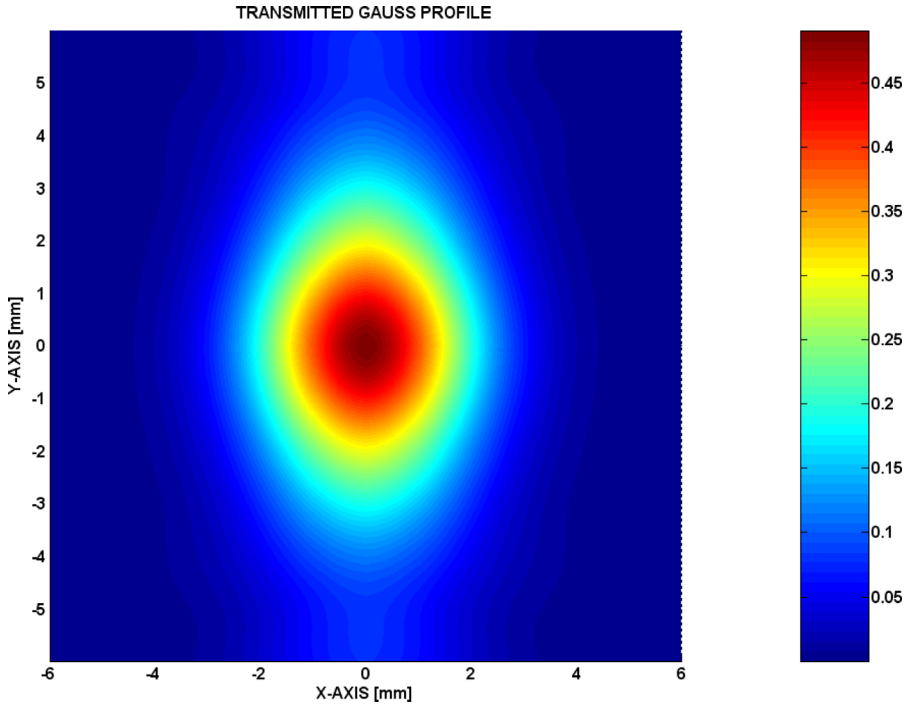

Fig. 4. Transmitted beam profile for an incident *Gaussian beam* with the same energy as a *conical-like beam* for $\beta = 400/\mathrm{m}$. Note that the profile along the X-direction differs from the one along the Y-direction. The anisotropic disk does not significantly alter the *Gaussian beam* in any case.

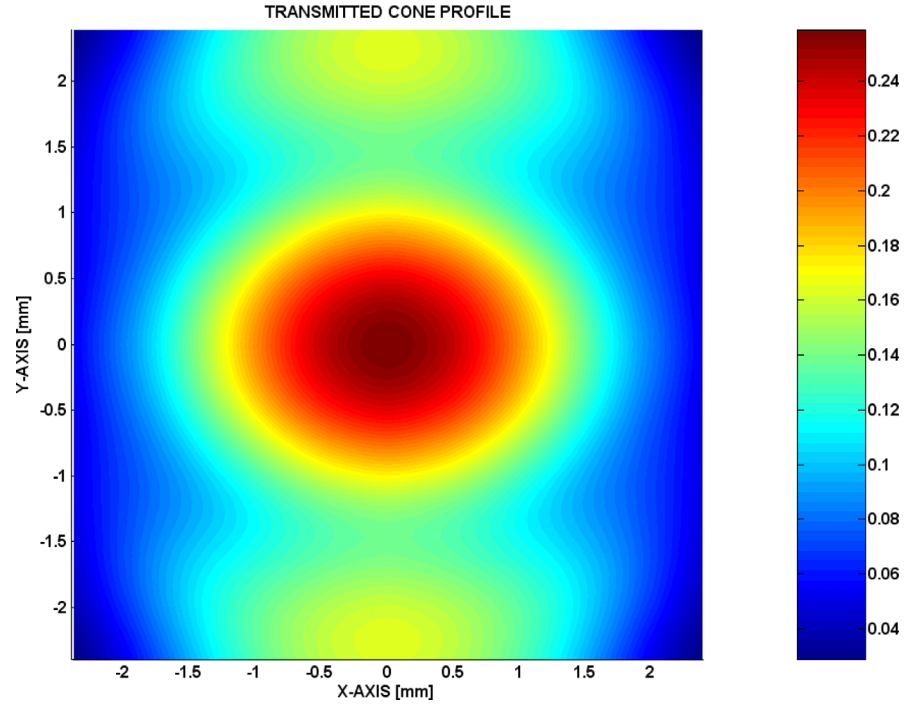

Fig. 5. Transmitted beam profile for a normal incident *conical-like beam* $\beta = 1000/\mathrm{m}$. There is a significant difference between the profile along the X-direction and the Y-direction.

conical-like beam for $\beta = 400/\mathrm{m}$. Note that the profile along the X-direction differs from the one along the Y-direction. A similar effect, caused by the anisotropic disk, was found for the reflected beam, though less outspoken and less useful for the applications the topic of this paper aims at. The *Gaussian beam* is not very much influenced by the anisotropic disk, though comparing results for the other profiles are appealing.

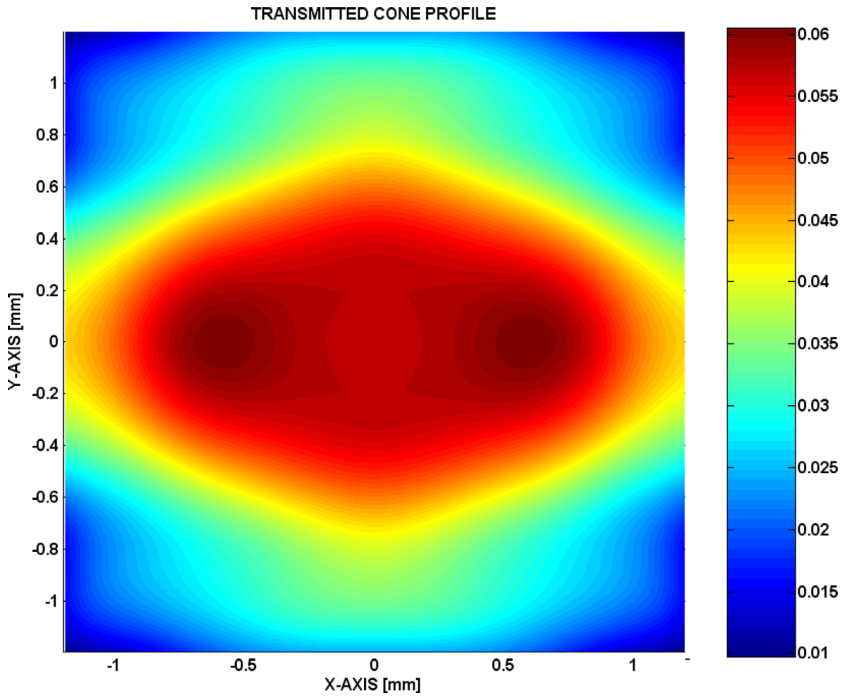

Fig. 6. Transmitted beam profile for a normal incident *conical-like beam* $\beta = 2000/\text{m}$. The pattern is much different from the one in Figure 5.

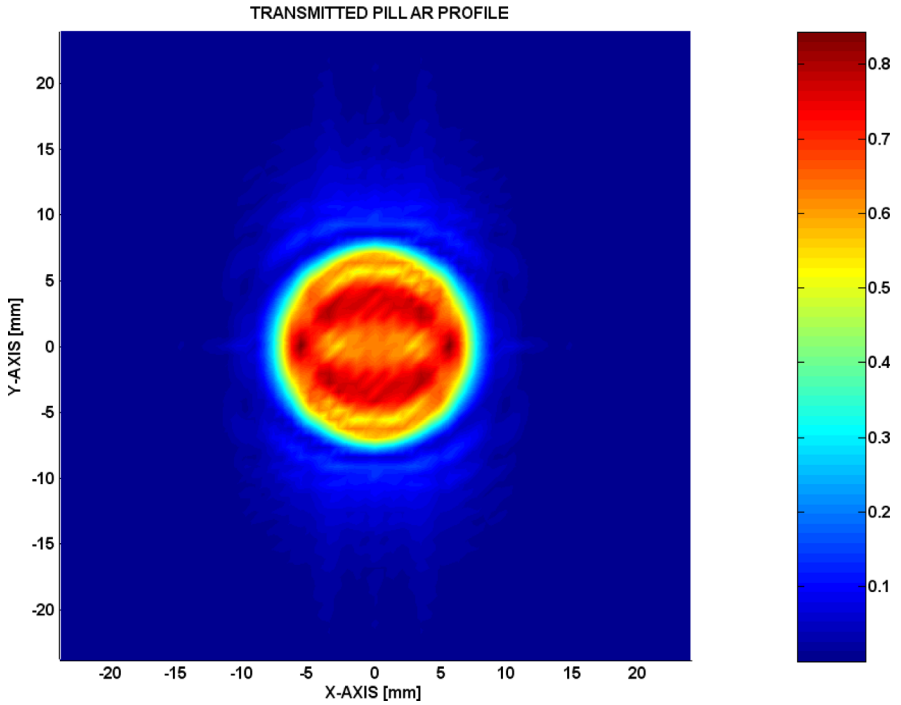

Fig. 7. Transmitted beam profile for an incident *pillar beam* having the same amount of energy as a *conical-like* beam for $\beta = 100/\text{m}$. The transmitted beam pattern is direction dependent for this type of beam, even for a relatively large diameter.

Figure 5 depicts the transmitted beam profile for a perpendicular incident *conical-like beam* $\beta = 100/\text{m}$. A significant difference exists between the profile along the X-direction and the Y-direction. Numerous simulations show that the *conical-like beam* profile is always more sensitive than the *Gaussian beam*. The reason must be that *conical-like beams* have an exponentially decaying amplitude, similar to inhomogeneous waves [63]. Indeed, the

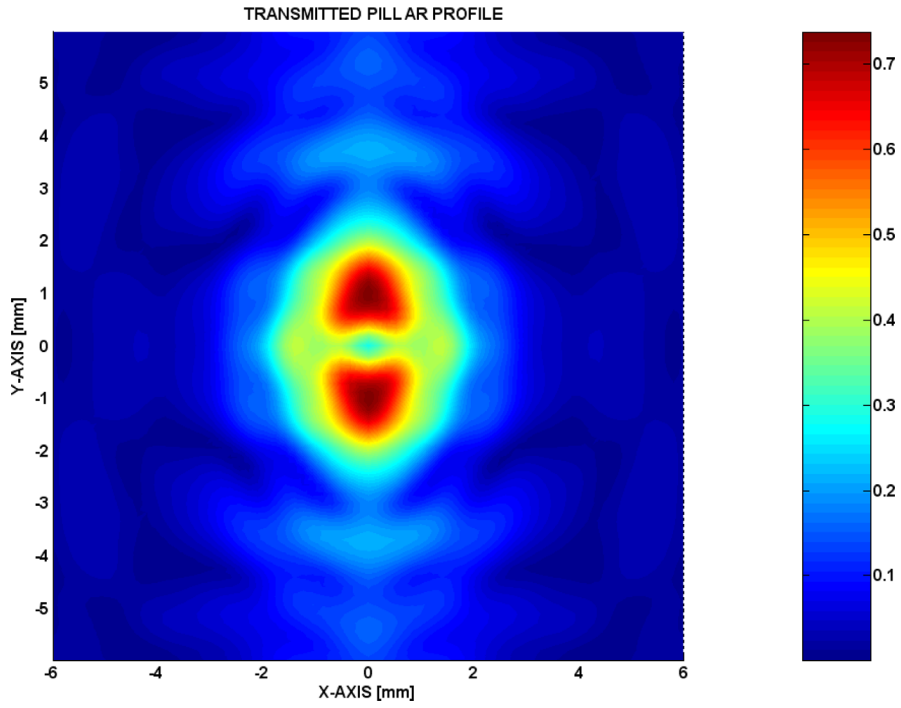

Fig. 8. Transmitted beam profile for an incident *pillar beam* with the same energy as a *conical-like beam* for $\beta = 400/\mathrm{m}$. The pattern is more outspoken than in Figure 7. The difference with Figure 4 is significant.

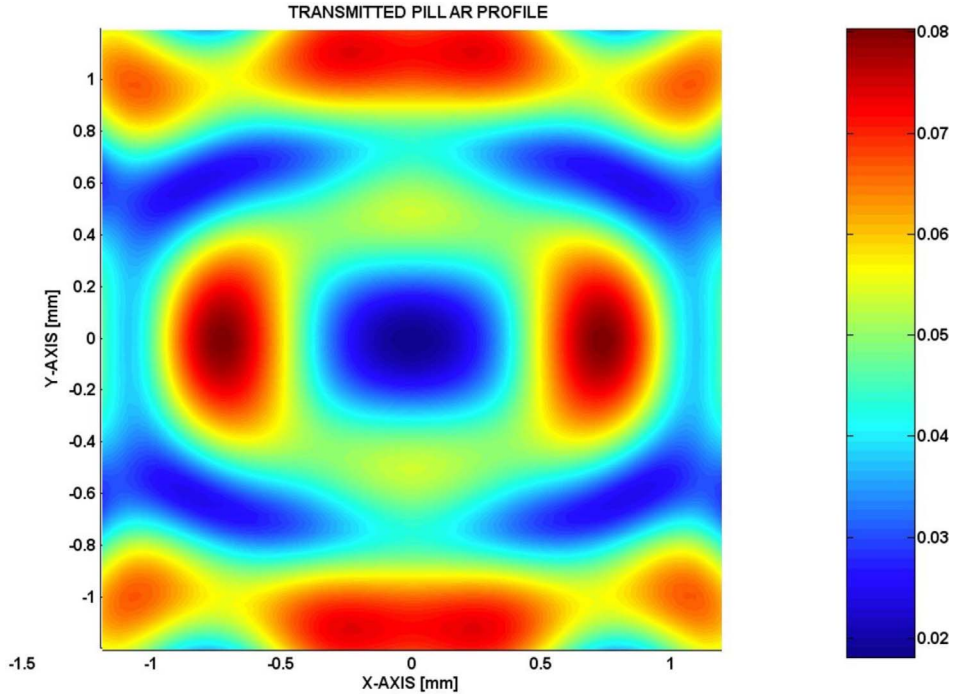

Fig. 9. Transmitted beam profile for an incident *pillar beam* having the same amount of energy as a *conical-like beam* for $\beta = 2000/\mathrm{m}$. The transmitted beam profile has a complicated shape and depends on the direction. The difference with Figure 6 is significant.

scattering and propagation of inhomogeneous waves depend also on the inhomogeneity vector's direction relative to the fiber direction [14].

If we increase the inhomogeneity β, as in Figure 6, where the transmitted beam profile for a perpendicularly incident *conical-like beam*, $\beta = 2000/\mathrm{m}$, is given, we see that the pattern is much different from the one in Figure 5. This is because the scattering and propagation properties of inhomogeneous waves also depend on the magnitude of the inhomogeneity β. Another reason for the latter phenomenon is

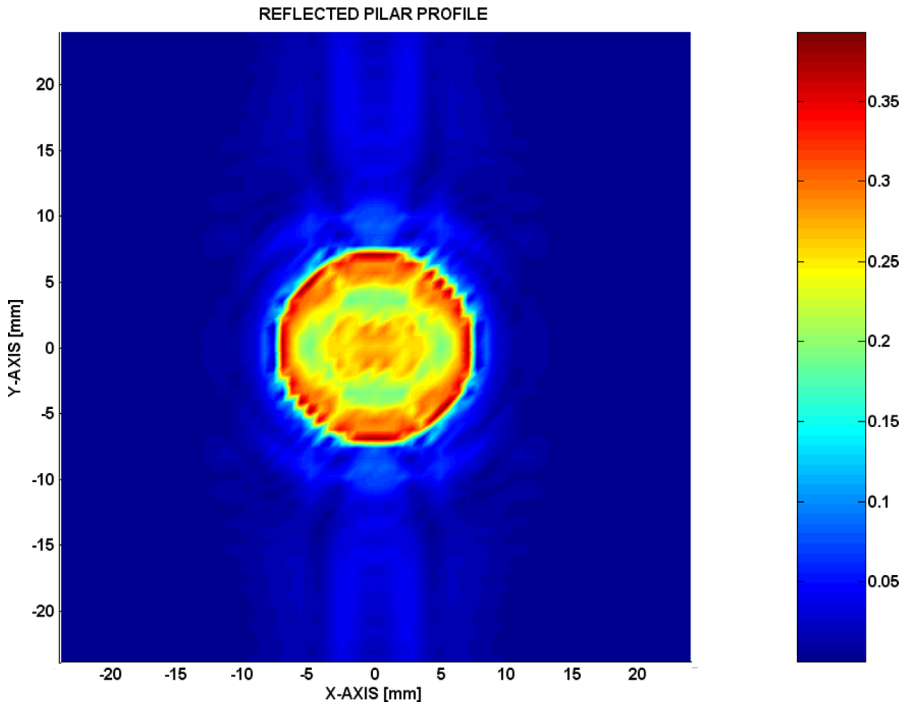

Fig. 10. Reflected beam profile for an incident *pillar beam* having the same amount of energy as a *conical-like* beam for $\beta = 100/\mathrm{m}$. The result can be compared with Figure 7 of the transmitted profile.

that narrower beams diffract much more, whence more propagation angles are involved, resulting in better sensitivity to the anisotropic elastic properties of the encountered material.

Because *conical-like beams* might be challenging to generate experimentally, we have also performed simulations for *pillar beams*, which are presumably easier to generate. We found that *pillar beams* are much more sensitive to material properties and fiber direction than classical *Gaussian beams*. Figure 7 depicts the transmitted beam profile for an incident *pillar beam* with the same energy as a *conical-like beam* for $\beta = 100/\mathrm{m}$. The transmitted beam pattern is direction-dependent for this type of beam, even for a relatively large diameter.

If we decrease the beam diameter, such as in Figure 8, where the transmitted beam profile for an incident *pillar beam* having the same amount of energy as a *conical-like beam* for $\beta = 400/\mathrm{m}$, is shown, the pattern becomes more outspoken, certainly if compared to Figure 4.

In extreme situations, such as in Figure 9 (to be compared with Fig. 6) where the transmitted beam profile for an incident *pillar beam* having the same amount of energy as a *conical-like beam* for $\beta = 2000/\mathrm{m}$, is shown, the transmitted beam profile has an even more complicated shape and depends very strongly on the direction in the XY-plane.

Finally, to show the capabilities of the applied simulations, Figure 10 exposes an example of a reflected field for normal incidence, matching the case of Figure 7, where the transmission was shown. A study of how this reflected field would interact with the metamaterial and transducer is beyond the scope of this feasibility study for transmission. Further investigations would require a complete investigation, including an emitting transducer, a metamaterial, and the anisotropic disk as one complex system.

4 Conclusions

The report shows that transmitted beam profiles change when transmitted through an anisotropic disk. Furthermore, *conical-like* and *pillar beams* are more influenced than *Gaussian beams*. Even though this feasibility study used one particular unidirectional fiber-reinforced composite layer as a model, depending on the requirements, the material can be tuned to match specific applications in which an anisotropic disk is placed in front of a single element transducer or a transducer covered by a metamaterial, to change transmitted beam characteristics further. Even though tunability may not be as sophisticated or flexible as a metasurface, its simplicity may add to the practical realization of specific beam profiles in a less expensive and lower level of fabrication sophistication than when only metamaterials are considered.

References

1. J. Kim, S. Kasoji, P.G. Durham, P.A. Dayton: Acoustic hologram lens made of nanoparticle-epoxy composite molding for directing predefined therapeutic ultrasound beams, in 2022 IEEE International Ultrasonics Symposium (IUS), Venice, Italy, 2022, pp. 1–4. https://doi.org/10.1109/IUS54386.2022.9957379.

2. S. Jimenez-Gambin, N. Jimenez, JM. Benlloch, F. Camarena: Holograms to focus arbitrary ultrasonic fields through the skull. Physical Review Applied 12, 1 (2019) 014016.
3. H. Ahmed, S. Ghosh, T. Sain, S. Banerjee: Hybrid Bessel beam and metamaterial lenses for deep laparoscopic nondestructive evaluation. Journal of Applied Physics 129, 16 (2021) 165107.
4. T. Yang, Y. Jin, T.-Y. Choi, N. Dahotre, A. Neogi; Mechanically tunable ultrasonic metamaterial lens with a subwavelength resolution at long working distances for bioimaging. Smart Materials and Structures 30, 1 (2021) 015022.
5. Y. Jin, R. Kumar, O. Poncelet, O. Mondain-Monval, T. Brunet: Flat acoustics with soft gradient-index metasurfaces. Nature Communications 10 (2019) 143.
6. H. Gao, X. Fang, Z. Gu, T. Liu, S. Liang, Y. Li, J. Zhu: Conformally mapped multifunctional acoustic metamaterial lens for spectral sound guiding and Talbot effect. Research (Wash DC) 2019 (2019) 1748537. https://doi.org/10.34133/2019/1748537.
7. Kun Li, Bin Liang, Jing Yang, Jun Yang, Jian-chun Cheng: Broadband transmission-type coding metamaterial for wavefront manipulation for airborne sound. Applied Physics Express 11, 7 (2018) 077301.
8. C. Shen, X. Jun, N.X. Fang, Y. Jing: Anisotropic complementary acoustic metamaterial for canceling out aberrating layers. Physical Review X 4, 4 (2014) 041033.
9. F. Semperlotti, H. Zhu: Achieving selective interrogation and sub-wavelength resolution in thin plates with embedded metamaterial acoustic lenses. Journal of Applied Physics 116, 5 (2014) 054906.
10. S. Yaacoubi, P. McKeon, W. Ke, N.F. Declercq, F. Dahmene: Towards an ultrasonic guided wave procedure for health monitoring of composite vessels: application to hydrogen-powered aircraft. Materials 10, 9 (2017) 1097. https://doi.org/10.3390/ma10091097.
11. M. Veidt, W. Sachse: Ultrasonic evaluation of thin, fiber-reinforced laminates. Journal of Composite Materials 28, 4 (1994) 329–342.
12. W.P. Rogers: Elastic property measurement using Rayleigh-Lamb waves. Research in Nondestructive Evaluation 6, 4 (1995) 185–208.
13. P.B. Nagy, A. Jungman, L. Adler: Measurements of backscattered leaky Lamb waves in composite plates. Materials Evaluation 46, 1 (1988) 97–100.
14. S. Eckel, F. Meraghni, P. Pomarede, N.F. Declercq: Investigation of damage in composites using nondestructive nonlinear acoustic spectroscopy. Experimental Mechanics 57 (2017) 207–17. https://doi.org/10.1007/s11340-016-0222-6.
15. D.E. Chimenti, J. Song: Performance of spherically focused air-coupled ultrasonictransducers. AIP Conference Proceedings 894 (2007) 862.
16. S.D. Holland, S.V. Teles, D.E. Chimenti: Quantitative air-coupled ultrasonic materials characterization with highly focussed acoustic beams. Review of Progress in Quantitative Nondestructive Evaluation 23a and 23b (2004) 1376–1381.
17. D. Fei, D.E. Chimenti, S.V. Teles: Material property estimation in thin plates using focused, synthetic-aperture acoustic beams. Journal of the Acoustical Society of America 113, 5 (2003) 2599–2610.
18. D.E. Chimenti, S.D. Holland, D. Fei: Air-coupled ultrasound and rapid elastic property characterization using focused acoustic beams. 2003 IEEE Ultrasonics Symposium Proceedings 1 and 2 (2003) 266–275.
19. S.D. Holland, S.V. Teles, D.E. Chimenti: Air-coupled, focused ultrasonic dispersion spectrum reconstruction in plates. Journal of the Acoustical Society of America 115, 6 (2004) 2866–2872.
20. A.H. Nayfeh, D. E. Chimenti: Propagation of guided waves in fluid-coupled plates of fiber-reinforced composite. Journal of the Acoustical Society of America 83, 5 (1988) 1736–1743.
21. W. Sachse, Y.H. Pao: Determination of phase and group velocities of dispersive waves in solids. Journal of Applied Physics 49, 8 (1978) 4320–4327.
22. M. Deschamps, B. Hosten: The effects of viscoelasticity on the reflection and transmission of ultrasonic-waves by an orthotropic plate. Journal of the Acoustical Society of America 91, 4 (1992) 2007–2015.
23. R.L. Weaver, W. Sachse, L. Niu: Transient ultrasonic-waves in a viscoelastic plate – applications to materials characterization. Journal of the Acoustical Society of America 85, 6 (1989) 2262–2267.
24. L. Satyanarayan, JM. Vander Weide, N.F. Declercq: Ultrasonic polar scan imaging of damaged fiber-reinforced composites, Materials Evaluation 68, 6 (2010) 733–739.
25. R. Raišutis, O. Tumšys: Application of dual focused ultrasonic phased array transducer in two orthogonal cross-sections for inspection of multi-layered composite components of the aircraft fuselage. Materials (Basel) 13, 7 (2020) 1689. https://doi.org/10.3390/ma13071689.
26. D. Hopkins, M. Datuin, M. Brassard: Challenges and solutions for ultrasonic phased-array inspection of polymer-matrix composites at production rates, in 45th Annual Review of Progress in Quantitative Nondestructive Evaluation vol. 38, AIP Conference Proceedings 2102, UNSP 100002-1, 2019.
27. D.W. Schindel: Ultrasonic imaging of solid surfaces using a focussed air-coupled capacitance transducer. Ultrasonics 35, 8 (1998) 587–594.
28. D.E. Chimenti, D. Fei: Scattering coefficient reconstruction in plates using focused acoustic beams. International Journal of Solids and Structures 39, 21–22 (2002) 5495–5513.
29. V.M. Levin, O.I. Lobkis, R.G. Maev: Investigation of the spatial structure of acoustic fields by a spherical focusing transducer. Soviet Physics Acoustics-USSR 36, 4 (1990) 391–395.
30. B. Hosten, D.A. Hutchins, D.W. Schindel: Measurement of elastic constants in composite materials using air-coupled ultrasonic bulk waves. Journal of the Acoustical Society of America 99, 4 (1996) 2116–2123.
31. A. Safaeinili, O.I. Lobkis, D.E. Chimenti: Air-coupled ultrasonic estimation of viscoelastic stiffnesses in plates. IEEE Transactions on Ultrasonics Ferroelectrics and Frequency Control 43, 6 (1996) 1171–1180.
32. N. Miqoi, P. Pomarede, N.F. Declercq, L. Guillaumat, G. Le Coz, S. Delalande, F. Meraghni: Detection and evaluation of barely visible impact damage in woven glass fabric reinforced polyamide 6.6/6 using ultrasonic imaging, X-ray tomography and optical profilometry. International Journal of Damage Mechanics 30 (2020) 323–348. https://doi.org/10.1177/1056789520957703.
33. P. Pomarède, L. Chehami, N.F. Declercq, F. Meraghni, J. Dong, A. Locquet, D.S. Citrin: Application of ultrasonic coda wave interferometry for micro-cracks monitoring in woven fabric composites. Journal of Nondestructive Evaluation, Springer Verlag 38, 1 (2019) 26–34.
34. J. Dong, P. Pomarede, L. Chehami, A. Locquet, F. Meraghni, N.F. Declercq, D.S. Citrin: Visualization of subsurface damage in woven carbon fiber-reinforced composites using polarization-sensitive terahertz imaging. NDT and E International 99 (2018) 72–79.
35. P. Pomarède, F. Meraghni, L. Peltier, S. Delalande, N.F. Declercq: Damage evaluation in woven glass reinforced polyamide 6.6/6 composites using ultrasound phase-shift analysis and X-Ray tomography. Journal of Nondestructive Evaluation 73, 12 (2018) 1–21.

36. A.-U. Rehman, C. Potel, J.-F. de Belleval: Numerical modeling of the effects on reflected acoustic field for the changes in internal layer orientation of a composite. Ultrasonics 36 (1998) 343–348.
37. C. Koch: Sound field measurement in a double layer cavitation cluster by rugged miniature needle hydrophones. Ultrasonics Sonochemistry 29 (2016) 439–446.
38. C. Koch, K.-V. Jenderka: Measurement of sound field in cavitating media by an optical fibre-tip hydrophone. Ultrasonics Sonochemistry 15, 4 (2008) 502–509.
39. J. Petelin, Z. Lokar, D. Horvat, R. Petkovsek: Localized measurement of a sub-nanosecond shockwave pressure rise time. IEEE Transactions on Ultrasonics Ferroelectrics and Frequency Control 69, 1 (2022) 369–376.
40. L. Jia, S. Chen, B. Xue, H. Wu, K. Zhang, X. Yang, Z. Zeng: Acoustic pressure measurement of pulsed ultrasound using acousto-optic diffraction. Proceedings of SPIE 10621 (2017) 75–84.
41. M.G. Moharam, L. Young: Criterion for Bragg and Raman-Nath diffraction regimes, Applied Optics 17, 11 (1978) 1757–1759.
42. A. Korpel: Visualization of cross section of a sound beam by Bragg diffraction of light. Applied Physics Letters 9, 12 (1966) 425–427.
43. A. Korpel: Proceedings of the Second International Symposium on Acoustical Holography. Plenum, London, England, 1970, p. 39.
44. A. Korpel: Acousto-Optics, 2nd ed. (Marcel Dekker Inc, New York, 1997, p. 21–22, 206–219.
45. K. Vandenabeele, M.A. Breazeale, O. Leroy, J.K. Na: Strong Interaction of arbitrary fields of sound and light – application to higher order Bragg Imaging. Journal of Applied Physics 75, 1 (1994) 84–95.
46. J.K. Na, M.A. Breazeale, O. Leroy: Ultrasonic Bragg imaging of flaws, Journal of the Acoustical Society of America 81, Suppl. 1 (1987) S43–S43.
47. L.H.V. Wang: Ultrasound-mediated biophotonic imaging: A review of acousto-optical tomography and photo-acoustic tomography. Disease Markers 19, 2–3 (2003) 123–138.
48. A. Teklu, N.F. Declercq, M. McPherson: Acousto-optic Bragg imaging of biological tissue. Journal of the Acoustical Society of America 136, 2 (2014) 634–637.
49. N.F. Declercq, M.S. McPherson, M.A. Breazeale, A.A. Teklu: Optical Bragg imaging of acoustic fields after reflection. Journal of the Acoustical Society of America 127, 6 (2010) 3466–3469.
50. NF Declercq, A. Teklu, M.A. Breazeale, R.D. Hasse, J. Degrieck, O. Leroy: Detection of fiber direction in composites by means of high frequency wide bounded ultrasonic beam and Schlieren photography. Research in Nondestructive Evaluation 16, 2 (2005) 55–64.
51. G. Cammi, A. Spinelli, F. Cozzi, A. Guardone: Automatic detection of oblique shocks and simple waves in Schlieren images of two-dimensional supersonic steady flows. Measurement 168 (2021) 108260.
52. H.D. Lim, X.F. Wei, B. Zang, U.S. Vevek, R. Mariani, T.H. New, Y.D. Cui: Short-time proper orthogonal decomposition of time-resolved Schlieren images for transient jet screech characterization. Aerospace Science and Technology 107 (2020) 106276.
53. E. Lampsijärvi, J. Heikkilä, I. Kassamakov, A. Salmi, E. Hæggström: Calibrated quantitative stroboscopic Schlieren imaging of ultrasound in air, in IEEE International Ultrasonics Symposium (IUS), Glasgow, UK 2019 (2019) 1651–1654. https://doi.org/10.1109/ULTSYM.2019.8925916.
54. Z. Xu, H. Chen, X. Yan, M.-L. Qian, Q. Cheng: Three-dimensional reconstruction of nonplanar ultrasound fields using Radon transform and the Schlieren imaging method. Journal of the Acoustical Society of America 142 (2017). EL82–EL88. https://doi.org/10.1121/1.4994282.
55. G. Caliano, A.S. Savoia, A. Iula: An automatic compact Schlieren imaging system for ultrasound transducer testing. IEEE Transactions on Ultrasonics Ferroelectric and Frequency Control 59, 9 (2012) 2102–2110. https://doi.org/10.1109/TUFFC.2012.2431.
56. M. Ohno, N. Tanaka, Y. Matsuzaki: Schlieren imaging by the interference of two beams in Raman-Nath diffraction. Japanese Journal of Applied Physics 42, 5b (2003) 3067–3071.
57. N.F. Declercq, R. Briers, J. Degrieck, O. Leroy: The history and properties of ultrasonic inhomogeneous waves. IEEE Transactions on Ultrasonics, Ferroelectrics, and Frequency Control 52, 5 (2005) 776–791. https://doi.org/10.1109/TUFFC.2005.1503963.
58. A.H. Naefeh: Wave propagation in layered anisotropic media with applications to composites, in North Holland series in Applied Mathematics and Mechanics, 1995.
59. S.I. Rokhlin, W. Wang: Double through-transmission bulk wave method for ultrasonic phase-velocity measurement and determination of elastic-constants of composite-materials. Journal of the Acoustical Society of America 91, 6 (1992) 3303–3312.
60. B. Hosten, M. Deschamps, B.R. Tittmann: Inhomogeneous wave generation and propagation in lossy anisotropic solids – application to the characterization of viscoelastic composite-materials. Journal of the Acoustical Society of America 82, 5 (1987) 1763–1770.
61. O.I. Lobkis, D.E. Chimenti, H. Zhang: In-plane elastic property characterization in composite plates. Journal of the Acoustical Society of America 107, 4 (2000) 1852–1858.
62. M. Deschamps, B. Hosten: The effects of viscoelasticiy on the reflection and transmission of ultrasonic waves by an orthotropic plate. Journal of the Acoustical Society of America 91, 4 (1992) 2007–2015.
63. N.F. Declercq: Experimental study of ultrasonic beam sectors for energy conversion into Lamb waves and Rayleigh waves. Ultrasonics 54, 2 (2013) 609–613.

Cite this article as: Declercq NF. 2023. Numerical study of beam shape adaptation by anisotropic disk covering transducer or metamaterial. Acta Acustica, **7**, 30.